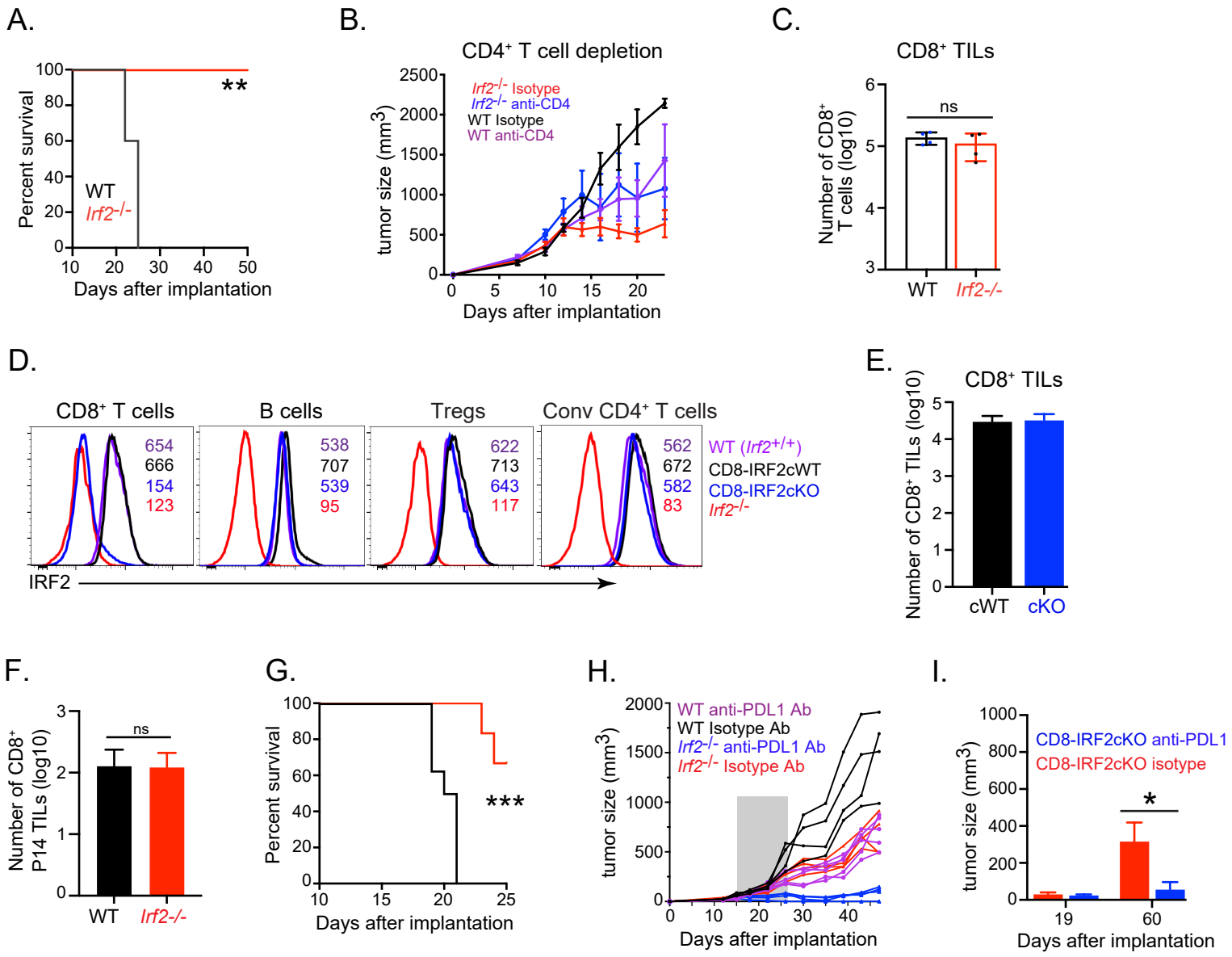
A.
Percent survival
100
80
60
40
20
0
10
20
30
40
50
Days after implantation
WT
Irf2-/-
**
B.
CD4+ T cell depletion
tumor size (mm3)
2500
2000
1500
1000
500
0
0
5
10
15
20
Days after implantation
Irf2-/- Isotype
Irf2-/- anti-CD4
WT Isotype
WT anti-CD4
C.
CD8+ TILs
Number of CD8+ T cells (log10)
6
5
4
3
ns
WT
Irf2-/-
D.
CD8+ T cells
B cells
Tregs
Conv CD4+ T cells
654
666
154
123
538
707
539
95
622
713
643
117
562
672
582
83
WT (Irf2+/+)
CD8-IRF2cWT
CD8-IRF2cKO
Irf2-/-
IRF2
E.
CD8+ TILs
Number of CD8+ TILs (log10)
5
4
3
2
1
0
cWT
cKO
F.
Number of CD8+ P14 TILs (log10)
3
2
1
0
ns
WT
Irf2-/-
G.
Percent survival
100
80
60
40
20
0
10
15
20
25
Days after implantation
***
H.
tumor size (mm3)
2000
1500
1000
500
0
0
10
20
30
40
Days after implantation
WT anti-PDL1 Ab
WT Isotype Ab
Irf2-/- anti-PDL1 Ab
Irf2-/- Isotype Ab
I.
tumor size (mm3)
1000
800
600
400
200
0
19
60
Days after implantation
CD8-IRF2cKO anti-PDL1
CD8-IRF2cKO isotype
*

Figure S1. Tumor growth, IRF2 expression and immunotherapy in WT and *Irf2*$^{-/-}$ mice, Related to Figures 1 and 2.

(A) Graph showing survival kinetics of WT (black) and *Irf2*$^{-/-}$ (red) mice implanted with MC38 tumors.

(B) Tumor growth kinetics in WT or *Irf2*$^{-/-}$ mice that received isotype control or anti-CD4 depleting antibody one day before MC38 tumor implantation.

(C) Graph shows the number of WT and *Irf2*$^{-/-}$CD8^{+} TILs from mice implanted with MC38 tumors.

(D) Flow plots show level of IRF2 expression in various immune cells from spleens of WT control (purple), CD8-IRF2cWT (IRF2 sufficient mice, black), CD8-IRF2cKO (IRF2-deficient only in CD8^{+} T cells, blue) and *Irf2*$^{-/-}$ (red) mice upon completion of a tumor kinetic study.

(E) Graph showing the number of CD8-IRF2cWT (WT) and CD8-IRF2cKO (cKO) CD8^{+} TILs from mice implanted with MC38 tumors.

(F) Graph depicting the number of tumor-specific (P14s) WT and *Irf2*$^{-/-}$CD8^{+} TILs from mice implanted with MC38 tumors.

(G) Graph showing survival kinetics of WT and *Irf2*$^{-/-}$ mice implanted with MC38 tumors.

(H) Individual mouse tumor growth kinetics in WT or *Irf2*$^{-/-}$ mice with orthotopic PyMT breast tumor cells that were treated with isotype or anti-PDL1 blocking antibody beginning on day 15 after tumor implantation.

(I) Tumor growth kinetics in CD8-IRF2cKO mice with orthotopic PyMT breast tumor cells that were treated with isotype or anti-PDL1 blocking antibody beginning on day 19 after implantation.

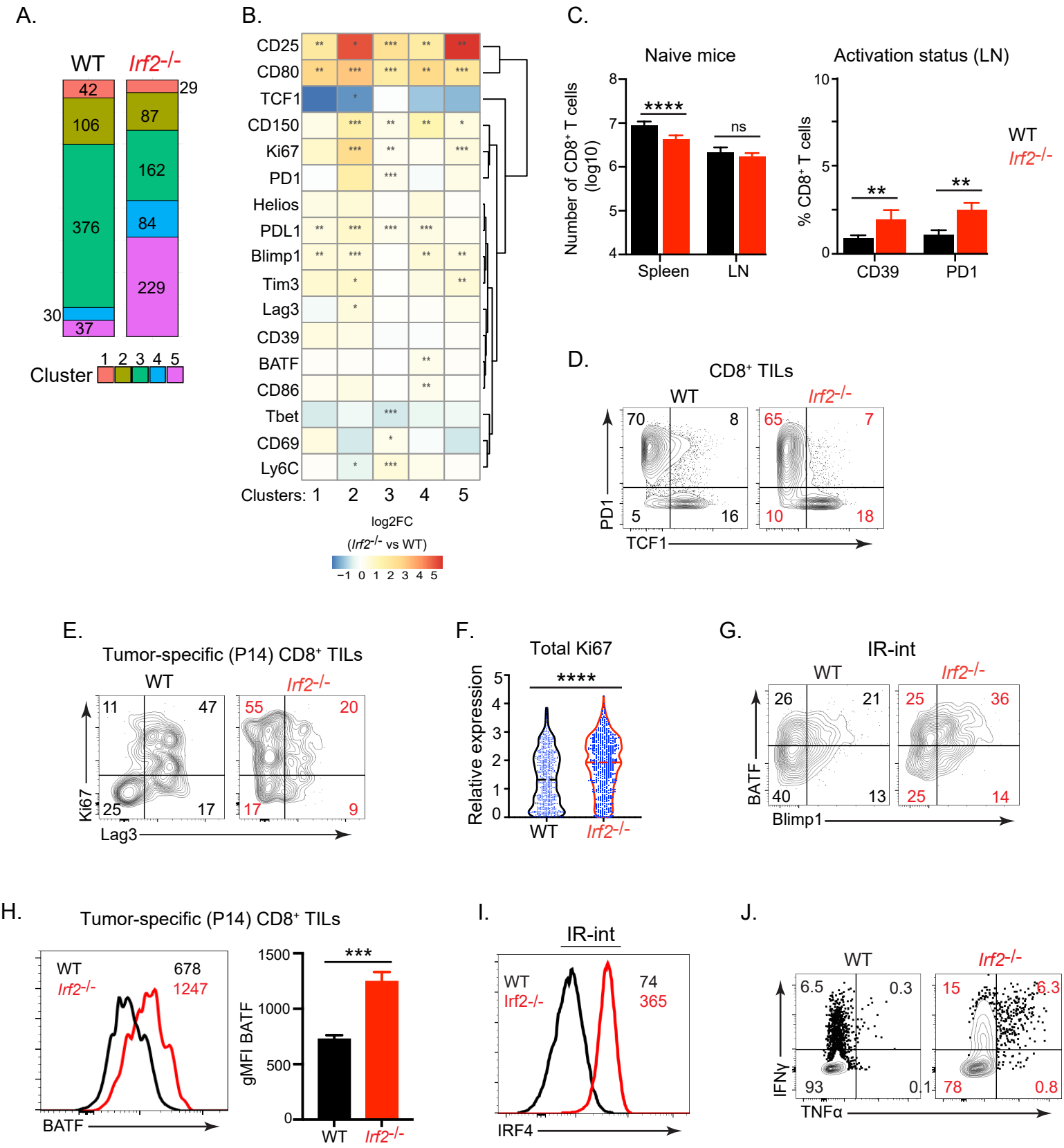
A.
WT
Irf2-/-
42
106
376
30
37
29
87
162
84
229
1 2 3 4 5
Cluster
B.
CD25
CD80
TCF1
CD150
Ki67
PD1
Helios
PDL1
Blimp1
Tim3
Lag3
CD39
BATF
CD86
Tbet
CD69
Ly6C
Clusters: 1 2 3 4 5
log2FC
(Irf2-/- vs WT)
−1 0 1 2 3 4 5
C.
Naive mice
Number of CD8+ T cells (log10)
****
ns
Spleen
LN
Activation status (LN)
% CD8+ T cells
**
**
CD39
PD1
WT
Irf2-/-
D.
CD8+ TILs
WT
Irf2-/-
70
8
5
16
65
7
10
18
PD1
TCF1
E.
Tumor-specific (P14) CD8+ TILs
WT
Irf2-/-
11
47
25
17
55
20
17
9
Ki67
Lag3
F.
Total Ki67
Relative expression
****
WT
Irf2-/-
G.
IR-int
WT
Irf2-/-
26
21
40
13
25
36
25
14
BATF
Blimp1
H.
Tumor-specific (P14) CD8+ TILs
WT
Irf2-/-
678
1247
BATF
gMFI BATF
***
WT
Irf2-/-
I.
IR-int
WT
Irf2-/-
74
365
IRF4
J.
WT
Irf2-/-
6.5
0.3
93
0.1
15
6.3
78
0.8
IFNγ
TNFα

Figure S2. Immune inhibitory and stimulatory protein expression in WT and *Irf2*$^{-/-}$ CD8^{+} TILs, Related to Figure 3.

(A) Bar graph depicts the number of MC38-infiltrating CD8^{+} T cells in each cluster in their respective WT and *Irf2*$^{-/-}$ groups. A total of 591 cells were analyzed in each group.

(B) Heatmap depicting log2FoldChange (*Irf2*$^{-/-}$ vs WT) of differentially expressed proteins between the WT and *Irf2*$^{-/-}$ CD8^{+} TILs within the same cluster. Red indicates increased in *Irf2*$^{-/-}$ and blue indicates increased in WT.

(C) The graphs indicated the number of naïve CD8^{+} T cells from the spleens and lymph nodes (LN) of WT and *Irf2*$^{-/-}$ mice, as well as the proportions of dLN CD8^{+} T cells expressing the indicated protein markers of immune activation.

(D) Flow plots indicating PD1 and TCF1 expression in WT and *Irf2*$^{-/-}$CD8^{+} TILs.

(E) Flow plots indicating Ki67 and Lag3 expression in tumor-specific (P14) WT and *Irf2*$^{-/-}$CD8^{+} TILs.

(F) Violin plot showing total Ki67 expression in WT and *Irf2*$^{-/-}$CD8^{+} TILs. Each blue dot represents a single cell.

(G) CyTOF plot showing BATF and Blimp1 expression by IR-int WT and *Irf2*$^{-/-}$ CD8^{+} T cells. The numbers in the plots indicate the percent of cells in each quadrant.

(H) Histogram showing BATF expression tumor-specific (P14) WT (black) and *Irf2*$^{-/-}$ (red) CD8^{+} TILs. The numbers in the histograms show the gMFI of BATF expression. The graph summarizes gMFI of BATF expression of tumor-specific CD8^{+} TILs from five mice.

(I) Histogram showing IRF4 expression by IR-int WT (black) and *Irf2*$^{-/-}$ (red) CD8^{+} TILs. The numbers in the histograms show the gMFI of IRF4 expression.

(J) Flow plots indicating IFNγ and TNFα co-expression in GP_{33-41} peptide stimulated WT and *Irf2*$^{-/-}$CD8^{+} TILs. The numbers in the plots show the percent of cells in each quadrant.

Data are representative of at least three independent experiments. In each experiment, tumors from 4 – 7 mice were pooled from each group (WT or *Irf2*$^{-/-}$) in order to obtain sufficient numbers of CD8^{+} TILs for analysis. * $p<0.05$, ** $p<0.01$, *** $p<0.001$, **** $p< 0.0001$.

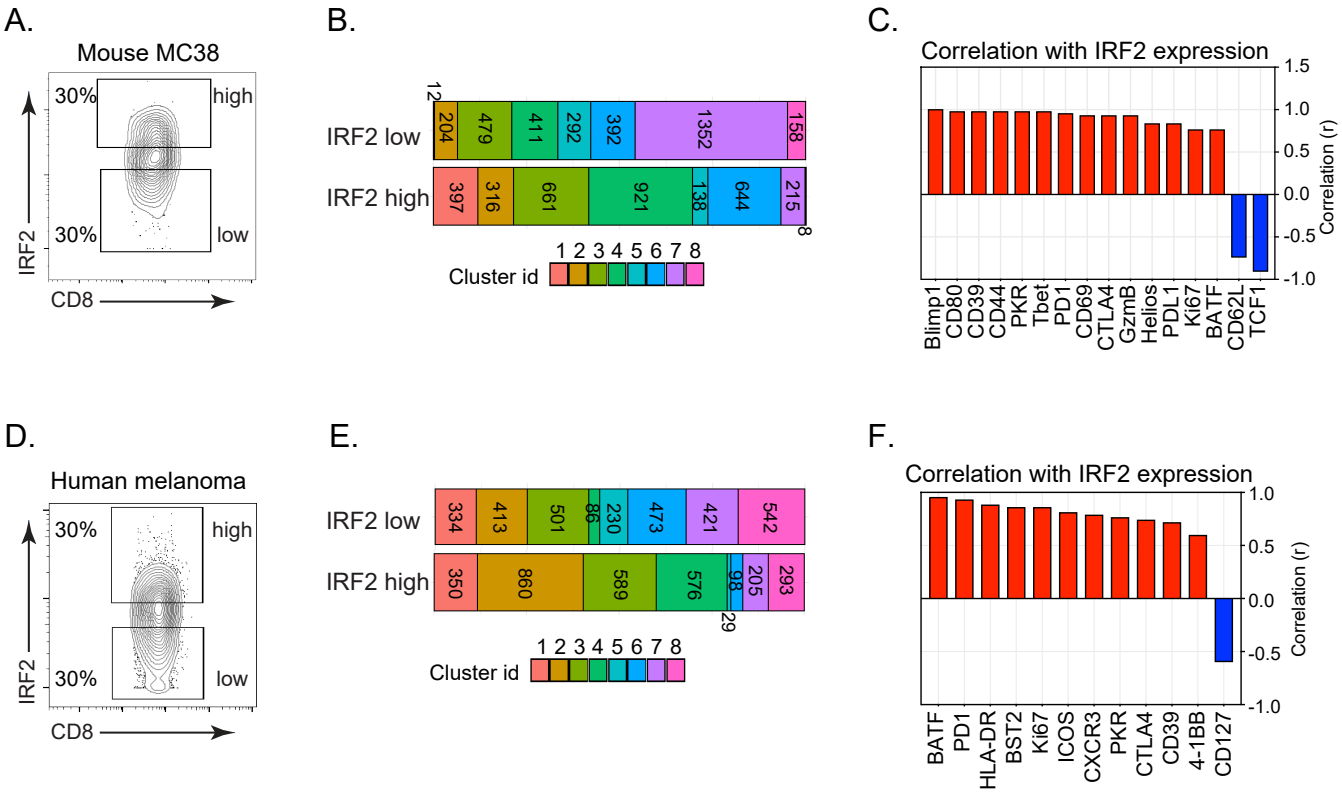
A.
Mouse MC38
30%
high
30%
low
IRF2
CD8
B.
IRF2 low
IRF2 high
12
204
479
411
292
392
1352
158
397
316
661
921
138
644
215
8
1 2 3 4 5 6 7 8
Cluster id
C.
Correlation with IRF2 expression
1.5
1.0
0.5
0.0
-0.5
-1.0
Correlation (r)
Blimp1
CD80
CD39
CD44
PKR
Tbet
PD1
CD69
CTLA4
GzmB
Helios
PDL1
Ki67
BATF
CD62L
TCF1
D.
Human melanoma
30%
high
30%
low
IRF2
CD8
E.
IRF2 low
IRF2 high
334
413
501
86
230
473
421
542
350
860
589
576
98
205
293
29
1 2 3 4 5 6 7 8
Cluster id
F.
Correlation with IRF2 expression
1.0
0.5
0.0
-0.5
-1.0
Correlation (r)
BATF
PD1
HLA-DR
BST2
Ki67
ICOS
CXCR3
PKR
CTLA4
CD39
4-1BB
CD127

Figure S3. IRF2 relationship to activation and IFN stimulated genes, Related to Figure 4.

(A) Bar graph depicts the number of MC38-infiltrating $CD8^+$ T cells in each cluster in their respective IRF2 high and IRF2 low groups. A total of 3300 cells were analyzed in each group.

(B) CyTOF plot showing gating of IRF2 high and IRF2 low fractions in MC38 $CD8^+$ TILs .

(C) Bar plots show Spearman correlation (r) of IRF2 with the indicated protein in MC38-infiltrating $CD8^+$ T cells

(D) Bar graph depicts the number of human melanoma-infiltrating $CD8^+$ T cells in each cluster in their respective IRF2 high and IRF2 low groups. A total of 3000 cells were analyzed in each group.

(E) CyTOF plot showing gating of IRF2 high and IRF2 low fractions in human melanoma $CD8^+$ TILs . The flow plots show one representative tumor from the five melanoma samples.

(F) Bar plots show Spearman correlation (r) of IRF2 with the indicated protein in human melanoma $CD8^+$ TILs.

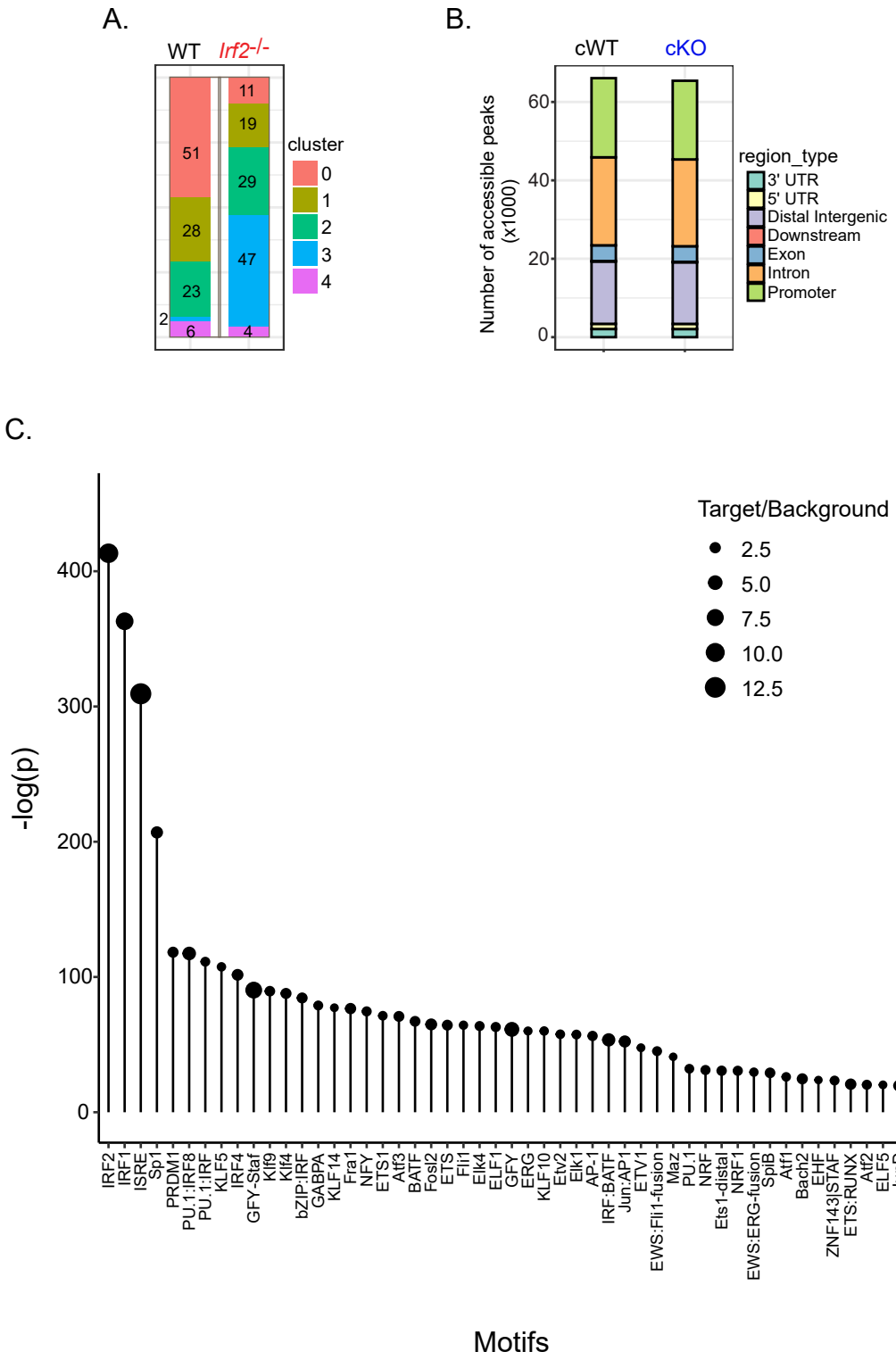
A.
WT
Irf2-/-
51
28
23
2
6
11
19
29
47
4
cluster
0
1
2
3
4
B.
cWT
cKO
Number of accessible peaks (x1000)
60
40
20
0
region_type
3' UTR
5' UTR
Distal Intergenic
Downstream
Exon
Intron
Promoter
C.
Target/Background
2.5
5.0
7.5
10.0
12.5
-log(p)
400
300
200
100
0
IRF2
IRF1
ISRE
Sp1
PRDM1
PU.1:IRF8
PU.1:IRF
KLF5
IRF4
GFY-Staf
Klf9
Klf4
bZIP:IRF
GABPA
KLF14
Fra1
NFY
ETS1
Atf3
BATF
Fosl2
ETS
Fli1
Elk4
ELF1
GFY
ERG
KLF10
Etv2
Elk1
AP-1
IRF:BATF
Jun:AP1
ETV1
EWS:Fli1-fusion
Maz
PU.1
NRF
Ets1-distal
NRF1
EWS:ERG-fusion
SpiB
Atf1
Bach2
EHF
ZNF143|STAF
ETS:RUNX
Atf2
ELF5
JunD
Motifs

Figure S4. Transcriptional and epigenetic analysis of CD8$^+$ TILs, Related to Figure 5.

(A) Bar graph depicts the number of MC38-infiltrating CD8$^+$ T cells in each cluster in their respective WT and *Irf2*$^{-/-}$ groups. A total of 679 cells were used in the scRNA-seq data analysis. Data representation is downsampled to 110 cells for each group.

(B) Bar graph depicting the number of accessible peaks in each indicated region of CD8-IRF2cWT (WT) and CD8-IRF2cKO (cKO) CD8$^+$ TILs.

(C) Top transcription factor motifs enriched in IRF2 target peaks as determined by HOMER motif analysis. Target/Background is the enrichment of motifs in the target peaks divided by the enrichment of those motifs in a random Homer simulated *k*-mer background; i.e., the number of target-peaks that have the indicated motif divided by the number of background-peaks that have the same motif.